Monthly Notices of the ROYAL ASTRONOMICAL SOCIETY
MNRAS **450,** 1320–1332 (2015) doi:10.1093/mnras/stv676

The early phases of galaxy clusters formation in IR: coupling hydrodynamical simulations with GRASIL-3D

Gian Luigi Granato,[1★] Cinthia Ragone-Figueroa,[1,2] Rosa Domínguez-Tenreiro,[3] Aura Obreja,[3] Stefano Borgani,[1,4] Gabriella De Lucia[1] and Giuseppe Murante[1]

[1]*Istituto Nazionale di Astrofisica INAF, Osservatorio Astronomico di Trieste, Via Tiepolo 11, I-34131 Trieste, Italy*
[2]*Instituto de Astronomía Teórica y Experimental (IATE), Consejo Nacional de Investigaciones Científicas y Técnicas de la República Argentina (CONICET), Observatorio Astronómico, Universidad Nacional de Córdoba, Laprida 854, X5000BGR Córdoba, Argentina*
[3]*Depto. de Física Teórica, Universidad Autónoma de Madrid, E-28049 Cantoblanco Madrid, Spain*
[4] *Astronomy Unit, Department of Physics, University of Trieste, via Tiepolo 11, I-34131 Trieste, Italy*

Accepted 2015 March 25. Received 2015 March 17; in original form 2014 December 18

ABSTRACT

We compute and study the infrared and sub-mm properties of high-redshift ($z \gtrsim 1$) simulated clusters and protoclusters. The results of a large set of hydrodynamical zoom-in simulations including active galactic nuclei (AGN) feedback, have been treated with the recently developed radiative transfer code GRASIL-3D, which accounts for the effect of dust reprocessing in an arbitrary geometry. Here, we have slightly generalized the code to adapt it to the present purpose. Then we have post-processed boxes of physical size 2 Mpc encompassing each of the 24 most massive clusters identified at $z = 0$, at several redshifts between 0.5 and 3, producing IR and sub-mm mock images of these regions and spectral energy distributions (SEDs) of the radiation coming out from them. While this field is in its infancy from the observational point of view, rapid development is expected in the near future thanks to observations performed in the far-IR and sub-mm bands. Notably, we find that in this spectral regime our prediction are little affected by the assumption required by this post-processing, and the emission is mostly powered by star formation (SF) rather than accretion on to super massive black hole (SMBH). The comparison with the little observational information currently available, highlights that the simulated cluster regions never attain the impressive star formation rates suggested by these observations. This problem becomes more intriguing taking into account that the brightest cluster galaxies (BCGs) in the same simulations turn out to be too massive. It seems that the interplay between the feedback schemes and the star formation model should be revised, possibly incorporating a positive feedback mode.

Key words: hydrodynamics – radiative transfer – dust, extinction – galaxies: clusters: general – infrared: galaxies – submillimetre: galaxies.

1 INTRODUCTION

Galaxy clusters are fundamental probes for many questions of extragalactic astrophysics and cosmology, both from the observational as well as from the theoretical point of view (for a recent review see Kravtsov & Borgani 2012). Their properties are relatively well known at low redshift $\lesssim 1$. In particular, it has been assessed that the central regions of massive clusters are dominated by passive early-type galaxies. Their stellar populations are old, having formed at $z \gtrsim 2$. More debated and uncertain is the main epoch at which these stellar populations assembled into the single galactic units we see in the local Universe. Indeed, there seems to be some disagreement between the relatively important role of merging below $z \lesssim 1$ expected on the basis of recent theoretical computations (Guo et al. 2011; Johansson, Naab & Ostriker 2012), and some observational constraints (Stott et al. 2011; Lidman et al. 2012; Lin et al. 2013; Inagaki et al. 2015). Unsurprisingly, a proper theoretical understanding of this and other questions concerning the evolution of galaxy populations in clusters requires a treatment of the various processes driving it, such as star formation (SF), active galactic nuclei (AGN) activity, feedback and dynamical interactions at a much deeper level than presently feasible. Galaxy clusters over cosmic time are prime laboratories for these processes acting together, which results in a clear environmental dependence of the basic properties of galaxies, and of their evolutionary history.

★ E-mail: giangigranato@gmail.com

At $z \gtrsim 1$, a regime approaching the formation epoch of massive clusters, observational studies become more and more problematic and, as a consequence, scarce. The identification of clusters (or protoclusters, somewhat loosely defined as systems that exhibit a significant overdensity of galaxies, not yet gravitationally bound, but that may collapse to form a cluster at later time) becomes difficult, due both to increasing detection challenges and intrinsic rareness. Also, a detailed determination of the properties of their galaxies is progressively uncertain.

Nevertheless, the study of high-z clusters is now an active field of research, as testified by the fact that even the redshift barrier of $z = 1.5$ has been broken in the last few years, by means of mid-infrared or X-ray selection, albeit by just a handful of examples so far. These observations suggest that, while galaxy populations in the centres of massive clusters show little change out to $z \sim 1.5$ (Mei et al. 2009; Strazzullo et al. 2010), in higher redshifts clusters, intense star formation becomes common, even in the cores and in the most massive galaxies (Hilton et al. 2010; Tran et al. 2010; Hayashi et al. 2011; Santos et al. 2011, 2014, 2015; Dannerbauer et al. 2014; Fassbender et al. 2014). For instance, Tran et al. (2010), considering only the IR luminous galaxies in the core (projected distances <0.5 Mpc) of a *Spitzer*-selected cluster at $z = 1.62$, found that the star formation rate (SFR) surface density to be at least $1700\,\mathrm{M_\odot\,yr^{-1}\,Mpc^{-2}}$. This estimate has been later revised downward by Santos et al. (2014) to $990 \pm 120\,\mathrm{M_\odot\,yr^{-1}\,Mpc^{-2}}$, with a contribution from the brightest cluster galaxy (BCG) of $256 \pm 70\ \mathrm{M_\odot\,yr^{-1}}$. Santos et al. (2015) measured a strikingly high amount of star formation $\sim 1100\ \mathrm{M_\odot\,yr^{-1}}$ in the inner 250 kpc of a massive ($\sim 5 \times 10^{14}\,\mathrm{M_\odot}$) cluster at $z \sim 1.6$ Dannerbauer et al. (2014), using APEX LABOCA 870 μm observations of the field around the so-called spiderweb radio galaxy at $z = 2.16$, widely studied as a signpost for a massive cluster in formation, measured an SFR density of $\sim 900\ \mathrm{M_\odot\,yr^{-1}\,Mpc^{-3}}$, occurring within a region of 2 Mpc.[1] On the other hand, there are also examples of high-redshift clusters ($z \gtrsim 2$) with a mixed population comprising both quiescent, structurally evolved galaxies, as well as star forming ones (Gobat et al. 2013; Strazzullo et al. 2013), or even clusters dominated by quiescent early-type galaxies (Tanaka et al. 2013). In any case, there have been reports of a reversal of the SFR–density relation, showing increasing SFR with increasing local density at $z \gtrsim 1$, both in the field as well as in higher density environments (Elbaz et al. 2007; Cooper et al. 2008; Tran et al. 2010; Santos et al. 2014, 2015).

To shed light directly on the history of assembly of galaxy clusters, it is clear that larger samples are highly demanded at high redshift, greater than 1–1.5. Moreover, various samples should be selected by means of different techniques, in order to capture different evolutionary stages of clusters or protoclusters. A widely used method to discover high-redshift clusters has been to look for the effects of their hot gas component, namely its X-ray emission or the Sunyaev–Zel'dovich (SZ) effect it produces on the cosmic microwave background. The former type of selection becomes rapidly inefficient at $z \gtrsim 1.5$, due to sensitivity limitations, and both require massive and well-relaxed structures, whose number density is expected to be rapidly declining at such early cosmic epochs. A complementary possibility, which has been exploited in the past few years, is to pre-select overdensities of galaxies whose near-infrared photometric properties are characteristic of high redshift systems. These overdensities require later spectroscopic confirmation. At $z > 2$ most efforts have been devoted in the search of protoclusters using high-z giant radiogalaxies as tracers (e.g. Hatch et al. 2011; Dannerbauer et al. 2014; Rigby et al. 2014).

A recently explored alternative to select high-z clusters of galaxies has been used by Clements et al. (2014), taking advantage of the well-assessed efficiency of far-IR/sub-mm surveys in detecting high-z objects in a violent, dust obscured, star-forming phase (e.g. Coppin et al. 2006, and references therein). These authors, following the suggestion by Negrello et al. (2005), tested the idea of exploiting the all sky coverage of the *Planck* satellite survey, in order to detect candidate clusters undergoing a pristine and violent star-forming phase. These are expected to show up as cold compact sources, significantly contributing to the *Planck* number counts, which can be later confirmed as clumps of high-z galaxies by means of higher angular resolution maps produced by the *Herschel* satellite. In this first demonstrative study, Clements et al. (2014) uncovered four such sources looking just at the $\sim 90\ \mathrm{deg^2}$ of sky observed by *Herschel* as part of the HerMES survey.

The main purpose of this paper is to compare these findings with the predictions of our high-resolution simulations of the formation of massive galaxy clusters (e.g. Ragone-Figueroa et al. 2013; Planelles et al. 2014). To do this, we post-process the simulation results at high $z \gtrsim 1$ with GRASIL-3D (Domínguez-Tenreiro et al. 2014), a recently developed fully three-dimensional radiative transfer code, which computes the dust reprocessing of the primary photons emitted by stellar populations (or other sources), and it has been developed specifically to deal with the output of simulations. This post-processing is of course required in order to properly compare with observations at IR or sub-mm wavelengths. We discuss to what extent the spectrophotometric properties of the cluster region are robust against reasonable variations of GRASIL-3D assumptions, in the various spectral regions. We incorporate in GRASIL-3D a consistent treatment of the radiative effect of AGN activity (our simulations include AGN feedback), which allows us to predict its contribution to the emitted specific luminosity.

Besides GRASIL-3D a few other tools exist with similar capabilities, and have been coupled with simulation output, e.g.: the later version of SUNRISE (Jonsson, Groves & Cox 2010); RADISHE (Chakrabarti & Whitney 2009); ART2 (Li et al. 2008) and SKIRT (Camps & Baes 2015). All but GRASIL-3D, which uses ray-tracing and finite difference, use Monte Carlo techniques to follow the transfer of photons through the diffuse interstellar medium (ISM), and hence the dust re-emission. However, to the best of our knowledge, this is the first time that this post-processing has been applied to galaxy clusters as a whole.

This paper is organized as follows: Section 2 is devoted to a brief description of the simulations set, and contains references to previous papers, wherein all the details can be retrieved; in Section 3, the radiative code used to post-process the simulations, GRASIL-3D, is described, including a few modifications introduced specifically for the purposes of this paper; the results are presented and discussed in Section 4, and summarized in the final Section 5.

[1] The SFRs reported in this paragraph have been obtained assuming a relationship between the total IR luminosity and SFR. The calibration of this relationship depends on the assumed initial mass function (IMF), which in the original papers was Salpeter in some cases (Dannerbauer et al. 2014; Santos et al. 2015) and Chabrier in others (Tran et al. 2010; Santos et al. 2014). In the former case, it is a factor of ∼1.7 higher. For the sake of homogeneity, we have converted all the estimates to the latter IMF, which is the same used in our simulations.

2 THE SIMULATIONS

For this work, we used simulations of 24 Lagrangian regions extracted from a low-resolution *N*-body simulation within a cosmological box of $1\,h^{-1}$ Gpc comoving size. We assumed a flat Λ cold dark matter cosmology with the following parameters: matter density parameter $\Omega_{\rm m} = 0.24$; baryon density parameter $\Omega_{\rm b} = 0.04$; Hubble constant $h = 0.72$; normalization of the power spectrum $\sigma_8 = 0.8$; primordial power spectral index $n_{\rm s} = 0.96$. The Lagrangian regions surround the most massive haloes identified at $z = 0$ in the parent simulation, all having virial mass[2] of at least $10^{15}\,h^{-1}\,{\rm M}_{\odot}$ (e.g. Bonafede et al. 2011). Initial conditions for the hydrodynamical simulations have been created by increasing mass resolution within such regions, and adding the corresponding high-frequency Fourier modes from the linear power spectrum of the adopted cosmological model. In the mass of Dark Matter (DM) particles is $8.47 \times 10^8\,h^{-1}\,{\rm M}_{\odot}$, and the initial mass of each gas particle is $1.53 \times 10^8\,h^{-1}\,{\rm M}_{\odot}$.

Our simulations were performed using the TreePM-SPH GADGET-3 code, an improved version of GADGET-2 (Springel 2005). The force accuracy, in the high-resolution regions, is set by $\epsilon = 5\,h^{-1}$ kpc for the Plummer-equivalent softening parameter, fixed in comoving units at redshifts >2 and fixed in physical units in the redshift range $2 \le z \le 0$. When computing hydrodynamical forces, the minimum value attainable for the smoothed particle hydrodynamics (SPH) smoothing length of the B-spline kernel is set to half of the gravitational softening length.

The simulations used in this work include gas cooling, star formation, supernova (SN) feedback and AGN feedback. We adopted a Chabrier IMF (Chabrier 2003). For a detailed description of the sub-resolution models, we refer the reader to Ragone-Figueroa et al. (2013) and Planelles et al. (2014). In particular, the former paper contains a discussion of the prescriptions for the black hole (BH) feedback, which is based on the simple recipe put forward by Springel, Di Matteo & Hernquist (2005) and adopted in many simulations, with a few important modifications. These were necessary because the latter model was thought and calibrated for non-cosmological high-resolution simulations of merging galaxies. It is now well recognized that the sub-resolution prescriptions are sensitive to resolution, and as such they generally require re-calibration or even a deeper rethinking when the resolution is changed (see e.g. Crain et al. 2015). Indeed, we found that the recipes proposed by Springel et al. (2005) for the BH feedback leads, in the context of our significantly lower resolution cosmological simulations, to several unwanted and misleading effects, discussed in Ragone-Figueroa et al. (2013), such as unrealistic merging of distant super massive black hole (SMBH) particles or losses of the energy produced by accretion. Our approach there has been to introduce the minimal changes required to avoid unreasonable results.

Since some concepts of this modelling are used in Section 3, to help the reader we provide here a brief summary. The BHs are represented by means of collisionless particles, subject only to gravitational forces, and growing by accretion and merging. The accretion rate is given by the minimum between a Bondi accretion rate, modified by the inclusion of a multiplicative factor, and the Eddington limit. The former is loosely thought of as providing an estimate of how the gas available for accretion scales with the conditions in the BHs surroundings, while the Eddington limit ensures that the produced radiation pressure does not overcome gravity. When two BH particles are within the gravitational softening and their relative velocity is smaller than a fraction 0.5 of the sound velocity of the surrounding gas, we merge them. The accretion on to SMBHs produces an energy determined by a parameter $\epsilon_r = 0.2$, giving the fraction of accreted mass converted to energy. Another parameter $\epsilon_f = 0.2$ defines the fraction of this energy that is thermally coupled to the surrounding gas. As usual, we calibrated these parameters in order to reproduce the observed scaling relations of SMBH mass in spheroids at $z = 0$.

For the analysis presented in this paper, we identified cluster progenitors at several redshifts $z \le 3$. In particular, our sample has a median virial mass of $8 \times 10^{13}\,h^{-1}\,{\rm M}_{\odot}$ and $2 \times 10^{14}\,h^{-1}\,{\rm M}_{\odot}$ at $z = 2$ and 1, respectively. The corresponding median SFRs within the virial radii are of 800 and 500 ${\rm M}_{\odot}\,{\rm yr}^{-1}$.

2.1 Cluster selection and initial conditions

As described in full details in Bonafede et al. (2011), the 24 most massive clusters, in terms of the mass assigned by the adopted cluster identification algorithm Friend of Friends (Davis et al. 1985), have been selected in the parent simulations at $z = 0$. The re-simulations at higher resolution have been carried out using the *Zoomed Initial Conditions* technique (Tormen, Bouchet & White 1997). The HR regions allow us to identify other 50 less massive and interesting clusters, uncontaminated by low-resolution particles, which have been studied in several papers (e.g. Ragone-Figueroa et al. 2013; Planelles et al. 2014). However, here we focus only on the 24 originally selected ones, because they constitute a statistically well-defined sample, whose final virial mass is in the range between $\simeq 1$ and $3 \times 10^{15}\,h^{-1}\,{\rm M}_{\odot}$ (see table 1 in Bonafede et al. 2011). Our sample has a median virial mass of $8 \times 10^{13}\,h^{-1}\,{\rm M}_{\odot}$ and $2 \times 10^{14}\,h^{-1}\,{\rm M}_{\odot}$ at redshift 2 and 1, respectively, and the corresponding median SFRs within the virial radius are of 800 and 500 ${\rm M}_{\odot}\,{\rm yr}^{-1}$.

3 GRASIL-3D AND ITS MODIFICATIONS

In order to perform radiative transfer calculations in the region of simulated clusters, we use GRASIL-3D (Domínguez-Tenreiro et al. 2014), a recently developed fully three-dimensional radiative transfer code, which computes the dust reprocessing of the primary photons emitted by stellar populations (or other sources). GRASIL-3D, while largely based on the formalism of the widely used model GRASIL (Silva et al. 1998; Granato et al. 2000), has been specifically designed to be applied to systems with arbitrary geometry, in which radiative transfer through dust plays an important role, such as galaxies or interesting regions identified in the output of hydrodynamical galaxy formation codes. With respect to the already published version, we have introduced here a few modifications to adapt it to the output of our version of GADGET-3, in particular for what concerns the radiative effect of AGN activity. The main features of GRASIL-3D are summarized below, while we refer the reader to Domínguez-Tenreiro et al. (2014) for all the details. A description of the modifications introduced for the purposes of this paper follows this summary.

A somewhat overlooked point is that any sensible computation of radiative transfer from the output of cosmological simulations, inevitably requires the introduction of a few more free or uncertain parameters, with respect to those already demanded by the treatment of baryon physics in the simulation itself. These are related

[2] The virial radius and the virial mass are defined as the radius and the mass of the sphere encompassing a mean density equal to the overdensity of virialization, as predicted by the spherical collapse model, and for the cosmology adopted in this paper (Bryan & Norman 1998).

to the sub-resolution astrophysics, in particular that concerning the molecular clouds (MCs). Since MCs are the sites of star formation and massive stars spend part of their lives within or close to them, it is expected and well established that in star-forming systems, a significant fraction of dust reprocessing occurs precisely in MCs. This fraction is an increasing function of the specific star formation activity, and of the total reprocessing itself (e.g. Silva et al. 1998; Granato et al. 2000). Current cosmological hydrodynamical simulations that follow galaxy formation are only beginning to resolve MCs (we remind the reader that the typical sizes and masses of giant MCs are of the order of ∼10–20 pc and 10^5–10^6 $M_\odot$, respectively), for zoom-in simulations of single galaxies (e.g. Hopkins et al. 2014), but their high computational cost makes them un-doable as yet for simulations on cluster scales. Therefore some further sub-resolution modelling is required to cope with dust reprocessing.

In particular, in GRASIL-3D the ISM is divided into two components, the MCs and the diffuse *cirrus*. In order to calculate the mass in the form of MCs it is assumed that unresolved gas densities at any point of the simulated volume follow a lognormal probability distribution function (PDF), The mean of the PDF is given by the local gas density and dispersion σ (a free parameter), as suggested by small-scale (∼1 kpc) simulations. Then, the local contribution to the molecular fraction is given by the fraction of the PDF above a threshold density, $\rho_{\rm MC,thres}$. The two parameters introduced so far, which control the molecular gas fraction are, $\rho_{\rm MC,thres}$ and σ, may reasonably range from about 0.3 to 3 $M_\odot$ pc^{-3} and from 2 to 3, respectively.

Once the molecular fraction at any location of the system is calculated, GRASIL-3D takes into account the age-dependent dust reprocessing of stellar populations. This age dependence arises from the fact that younger stars are associated with denser ISM environments (note that GRASIL was the first model to take it into account). This is obtained assuming that stars younger than a certain time t_0 (a further parameter) are enshrouded within MCs, characterized by their mass $M_{\rm MC}$ and radius $R_{\rm MC}$. Then, the radiative transfer is treated separately in the two components with the required accuracy. We explicitly note that, even though we apparently introduced here two more parameters $M_{\rm MC}$ and $R_{\rm MC}$, what actually matters for the radiative transfer computation is the ratio $M_{\rm MC}/R^2_{\rm MC}$, which therefore should be regarded as the only new parameter. A detailed non-equilibrium calculation for dust grains smaller than a given radius (150 Å in this work) and for polycyclic aromatic hydrocarbons molecules (PAHs) is performed. Their emission is usually very important at $\lambda \lesssim 30$ µm in the cirrus component.

GRASIL-3D has a general applicability to the outputs of either Lagrangian or Eulerian hydrodynamic codes. The first applications of the code have been done interfacing it with the output of the P-DEVA and GASOLINE SPH codes (Domínguez-Tenreiro et al. 2014; Obreja et al. 2014).

The main modification of GRASIL-3D introduced in this work has been to account for the radiative effect of SMBH particles present in the simulation, which provide the AGN feedback as mentioned in Section 2. To do this, we assume that the radiation emitted by the SMBH particles is distributed according to a template spectral energy distribution (SED), properly normalized by the bolometric luminosity. The latter is computed from the accretion rate and from the radiative efficiency, as $L_{\rm bol} = \epsilon_r \dot{M} c^2$. We remind the reader that the former quantity is predicted by the simulation for each SMBH particle, while the efficiency ϵ_r is a parameter of the simulation. It is set to 0.2 in the runs used in this work (see Ragone-Figueroa et al. 2013, for details). As for the SED, we adopted in our standard computation the mean SED of SDSS quasars computed by Richards et al. (2006), plotted in Fig. 1. It is observationally known and theoretically expected that AGN are characterized by a substantial anisotropy of their emission, giving rise to the broad dichotomy between type 1 and type 2 AGN. This is likely related to a preferential axis in their central engine (for a recent review see Hoenig 2013). However, we neglect this complication here. This is owing to two reasons. The former is that our simulations do not give any prediction for the AGN preferential axis, which is possibly related to the SMBH spin. The second and most reassuring one is that we checked that different choices for the assumed template SED yields only very small differences in the predicted IR properties of clusters, which become usually negligible at $\lambda \gtrsim 100$ µm (see Section 4.2 and Fig. 5). This holds true even for the totally opposite case of assigning to all SMBH particles the typical SED of obscured type 2 QSO, such as that reported by Polletta et al. (2007), also shown in Fig. 1.

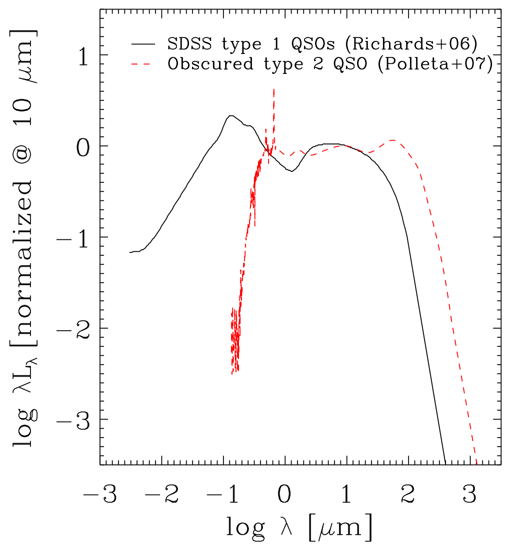

Figure 1. The SED templates adopted in this work to describe the emission of SMBH particles. In our standard computations, we used the mean SED of SDSS type 1 quasars by Richards et al. (2006, black solid line). To check the stability of our results on the IR properties of clusters, we used the very different typical SED of an obscured type 2 QSO, reported by Polletta et al. (2007, red-dashed line).

We note that these observational templates include by construction the reprocessing by dust in the region close to the SMBH, namely that which has been long since ascribed to a torus-like structure. The latter has been invoked to explain the observational differences between type 1 (*un-obscured*) and type 2 (*obscured*) AGNs (e.g. Pier & Krolik 1993; Granato & Danese 1994; Efstathiou & Rowan-Robinson 1995). This is actually what we need. Indeed, even though little can still be safely concluded on the detailed geometrical properties of these structures (e.g. Hoenig 2013, and references therein), even the more extended models do not consider torii larger than $\sim 200 (L_{\rm AGN}/(10^{46}\ {\rm ergs}^{-1}))^{1/2}$ pc (Granato, Danese & Franceschini 1997), which is far below the resolution of any cosmological simulation.

We assumed that SPH gas particles contain dust only when their temperature is lower than a certain threshold, that in this work we set to 10^5 Kelvin. However, the results are very weakly dependent on this value. For instance, we verified that the predicted SEDs of clusters are almost indistinguishable if the threshold is increased or decreased by a factor of ∼10. The maximum difference

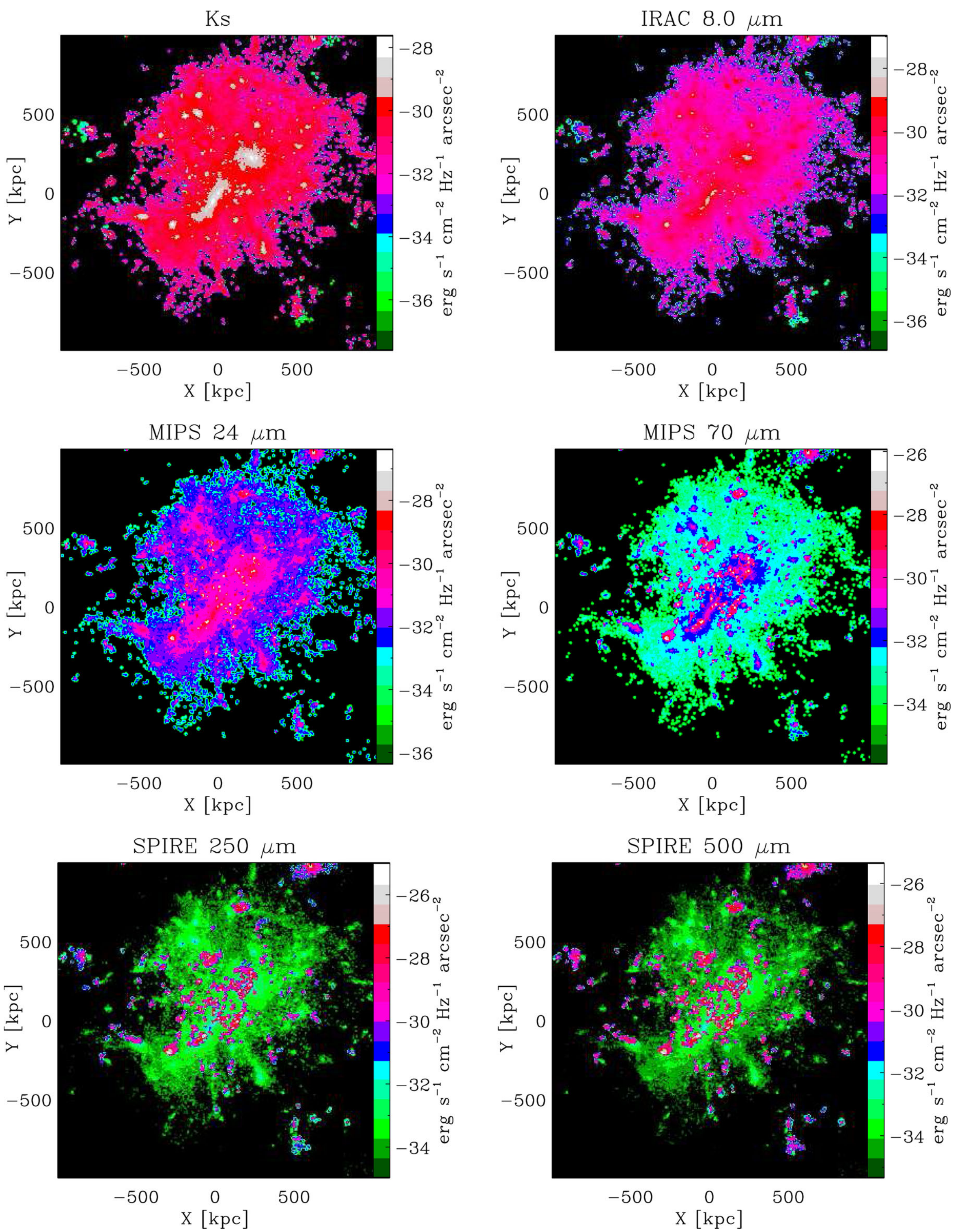

Figure 2. Examples of images of a cluster region at $z = 1$ produced by GRASIL-3D in various NIR to sub-mm bands. The physical size of each panel is 2000 kpc, close to the *Planck* HFI beam at that redshift. No telescope effects (like PSFs, pixel sizes, etc.) have been taken into account.

occurs at around the peak of dust emission $\sim 100\,\mu$m and in the far-UV, and is $\lesssim 10$ per cent. The dust to gas ratio δ of gas particles colder than the threshold temperature was assumed to be proportional to their metallicity, with a proportionality constant calibrated to get the standard galactic value 1/110 at solar metallicity, i.e. we set $\delta = Z/(110\,Z_{\odot})$. This corresponds to assuming that about 50 per cent of metals are locked in dust grains.

4 RESULTS

The outputs of GRASIL-3D are mock images of the portion of the simulated box in which the radiative transfer has been performed, and SEDs of the radiation coming out from the same box. We have processed boxes of physical size 2 Mpc, encompassing each of the 24 clusters, at several redshift between 0.5 and 3. Figs 2 and 3

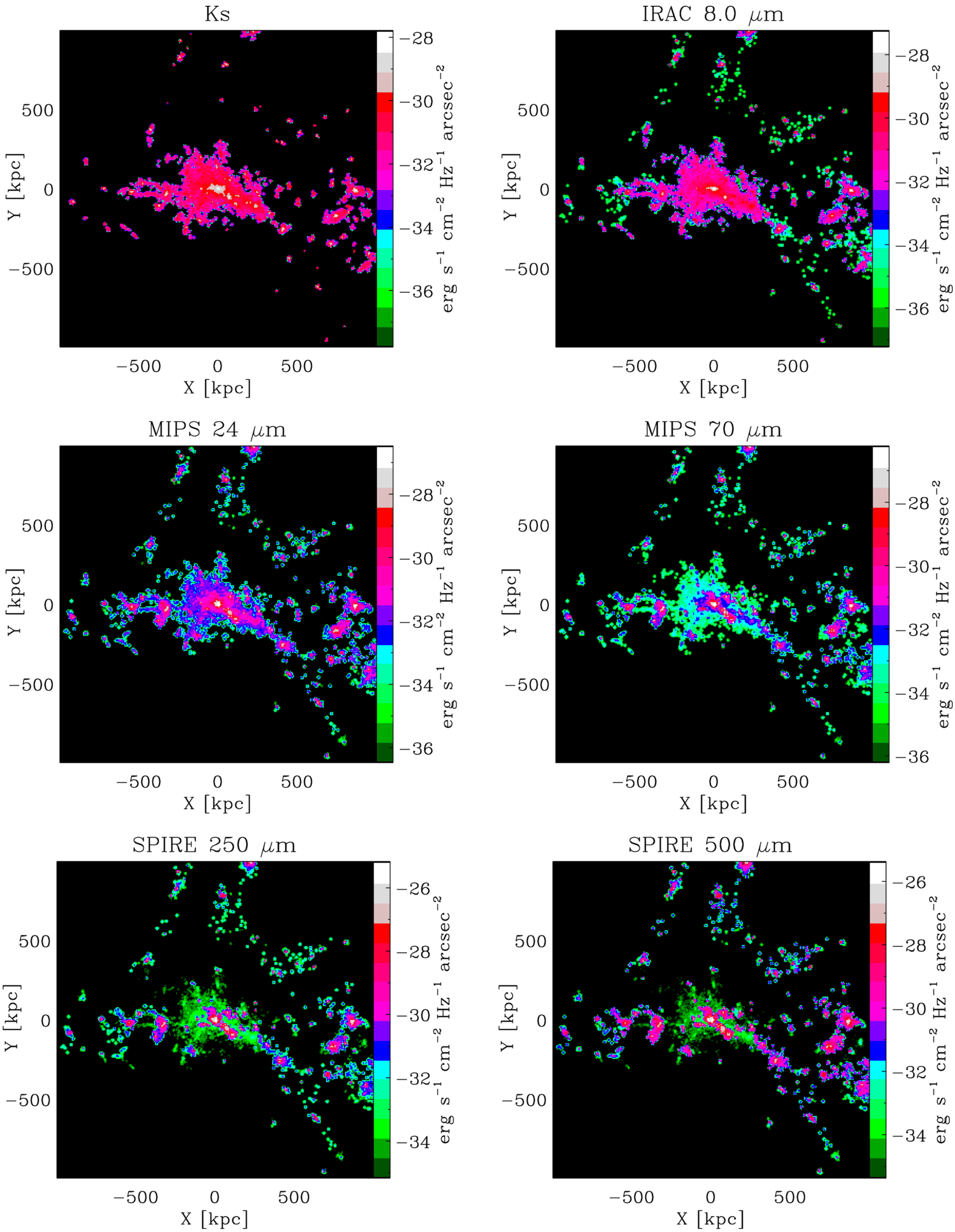

Figure 3. Same as Fig. 2 but at $z = 2$.

show examples of such images, in several interesting band-passes, for one of the clusters at redshift 1 and 2, respectively. The physical size of each panel is 2000 kpc, which at these redshift is close to the *Planck* High Frequency Instrument (HFI) beams ∼5 arcmin, and is larger than the virial diameter of the clusters at both redshifts, typically by a factor of ∼2 and 5, respectively. No telescope effects [like point spread functions (PSFs), pixel sizes, etc.] have been taken into account. In this Section, we will show how the predicted SEDs arising from the same region depend on GRASIL-3D parameters and other assumptions, and then we will discuss some implications for star forming cluster searches at sub-mm wavelengths.

4.1 Dependence on GRASIL-3D parameters and assumptions

To summarize, the parameters introduced by the radiative transfer calculations performed with GRASIL-3D are (i) the time-scale for newly born stars to get rid of the parent MC, t_0; (ii) the ratio between the mass of MCs and the square of their radius $M_{\rm MC}/R^2_{\rm MC}$, which in conjunction with the dust to gas ratio δ determines the optical depth of the MC, $\tau \propto \delta\, M_{\rm MC}/R^2_{\rm MC}$; we remind you that δ is set by the local gas metallicity, see end of Section 3; (iii) the threshold density for gas to be in the MC dense phase $\rho_{\rm mc,thres}$ and (iv) the dispersion σ of the sub-resolution PDF of gas densities. The latter two determines the fraction of gas in molecular form. Our adopted standard values for these quantities are reported in Table 1, together with their reasonable ranges (see Domínguez-Tenreiro et al. 2014, and references therein). Fig. 4 shows the SED of the same region of Fig. 2, computed under large variations of these parameters, with respect to our adopted standard values. These variations are thought to exacerbate the effects. Despite this, in the spectral region above ∼100 μm rest frame, which is that required to compare with the observations discussed in this paper, the effects are small, and become negligible above ∼200 μm. By converse at shorter IR wavelengths, where the contribution of MC becomes important, the consequences of these different choices of parameters may be significative, and would ask for careful evaluation. In particular, for $10 \lesssim \lambda \lesssim 40$ μm they may amount to a factor of ∼2.

Besides the uncertainties in GRASIL-3D outputs arising from the choice of its explicit parameters, there are also those related to the adopted optical properties of dust grains, which are by far less understood and predictable than commonly assumed (for a recent review see Jones 2014). In this work, we retain the same dust mixtures for the MCs and for the cirrus as in Domínguez-Tenreiro et al. (2014), which have been calibrated to reproduce the average properties of local galaxies. As for computing dust emission, the most delicate region is that below ∼30 μm, where the contribution from small thermally fluctuating grains and PAHs becomes important, and relatively minor variations just in the adopted size distribution of grains may produce large variations. This kind of uncertainty is expected to increase with redshift, and considering environments very different from those in which our knowledge of dust optical properties has been derived. At longer wavelengths, where the bulk of IR power is normally emitted, and is dominated by grains big enough to be in thermal equilibrium with the radiation field, the predictions are much more robust. Here, the largest source of uncertainty is possibly the wavelength decline of the grain absorption coefficient. The *canonical* computations by Draine & Lee (1984) used in this work yield a power-law decline $\propto \lambda^{-\beta}$ with $\beta = 2$ for $\lambda \gtrsim 40$ μm, however several laboratory measurements suggest a temperature dependence of β, with $1.5 < \beta < 2.5$ (see discussion and references in Jones 2014). Specifically, the possibility $\beta < 2$ has sometimes been welcomed, since it provides some minor help

Table 1. Parameters introduced by GRASIL-3D computation.

Parameter	Adopted value	Reasonable range	Short description
t_0	6 Myr	1–30 Myr	Escape time-scale of stars from parent MCs
$M_{\rm MC}/R^2_{\rm MC}$	$5\,10^5$ M$_\odot$/(10 pc)^2	10^5–10^6 M$_\odot$/(10 pc)^2	Determines MCs optical depth
$\rho_{\rm MC,thres}$	1 M$_\odot$/pc^3	0.3–3 M$_\odot$/pc^3	Threshold density for gas to be considered in MC phase
σ	2.5	2–3	Dispersion of the sub-resolution PDF of gas densities

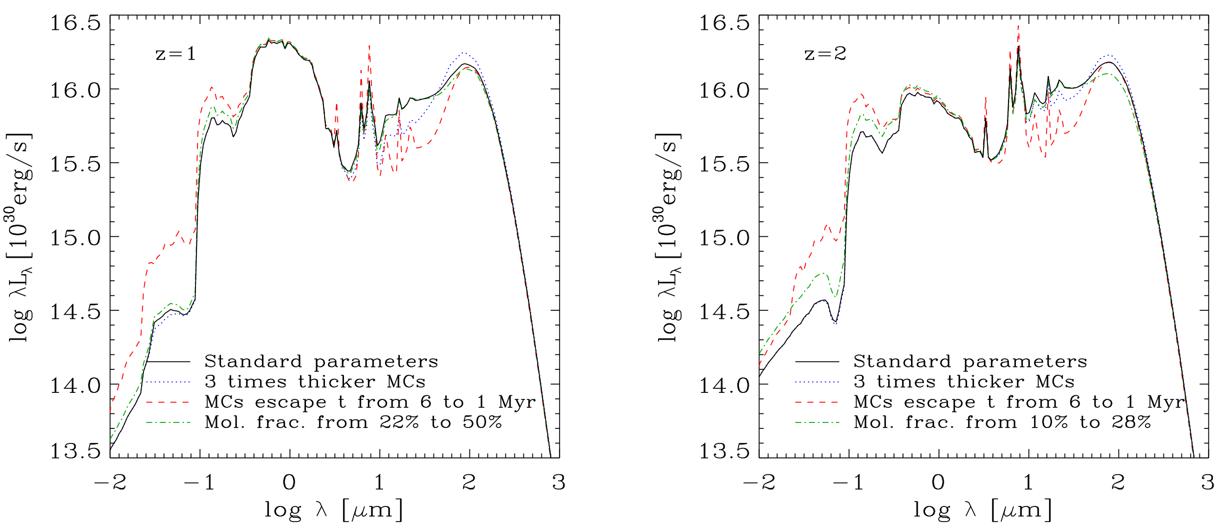

Figure 4. Comparison of the rest-frame SED obtained for one cluster at $z = 1$ and 2, with different choices of GRASIL-3D parameters. Solid black: standard values; blue-dotted: increasing the mass of individual MCs (and thus their optical depth) by a factor of 3; red dashed: decreasing the escape time-scale of stars from MC by a factor of 6 (from 6 to 1 Myr); green dot–dashed: decreasing the threshold for gas to be in the dense MC phase by a factor of 10, so that the molecular gas fraction increases from about 22 per cent to about 50 per cent at $z = 1$ and from about 10 per cent to 28 per cent at $z = 2$. In any case, the SEDs are very little affected above $\lambda \gtrsim 100$ μm, which is the spectral region on which we compare with observations in this paper. Note also that the parameter variations have been adopted to exacerbate the effects, but often leads to somewhat unrealistic values.

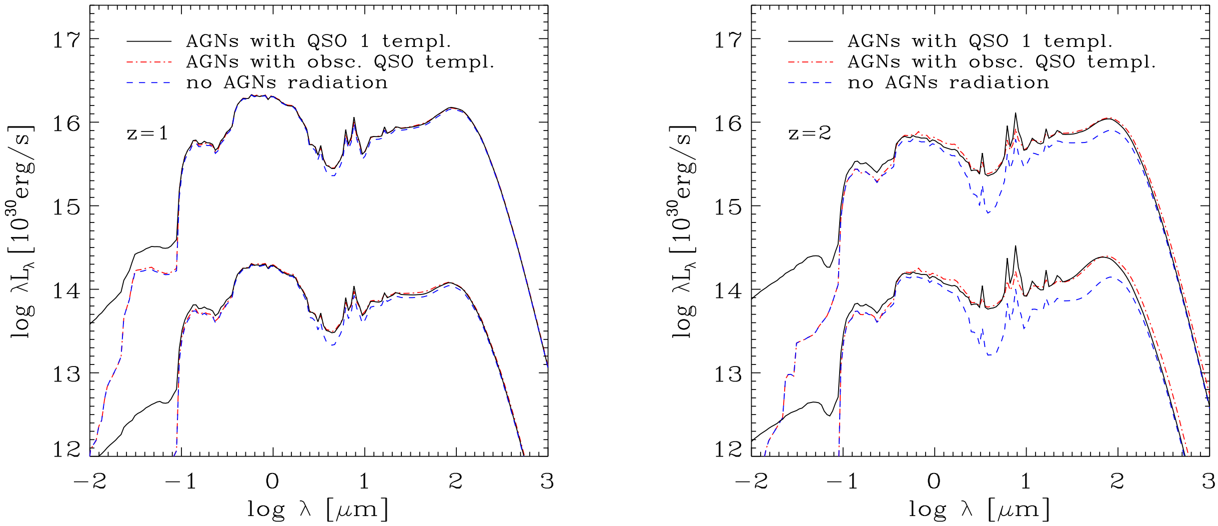

Figure 5. Comparison of the rest-frame SED obtained for two clusters at $z = 1$ and 2 by including or neglecting the radiative effect of AGNs, or by adopting different templates for it. The three lower lines have been artificially displaced by a factor of 10, and refer to a rare case (∼10 per cent at $z = 2$, but never at $z = 1$) in which the differences are most prominent (at $z = 2$), while the three upper lines refer to the same cluster considered in Fig. 4, which is more typical. Solid black: including the radiative effect of AGNs with our standard template, namely the mean SED of SDSS quasars by Richards et al. (2006); blue-dashed: neglecting the radiation emitted by AGNs; red dot–dashed: including the radiative effect of AGNs, but using the template by Polletta et al. (2007) for heavily obscured type 2 QSOs.

in the well-known difficulty of galaxy formation models in reproducing the high levels of bright sub-mm number counts (e.g. Baugh et al. 2005).

A detailed study of the dependence of IR properties of simulated clusters on dust properties is beyond the scope of this exploratory study. However, in view of the discussion of Section 4.3, which exploits the expected luminosity in the spectral range ∼100–400 μm rest frame, we checked that by adopting the extreme value $\beta = 1.5$ the SED is essentially unaffected below 100 μm. Above this wavelength the expected luminosity is progressively enhanced, typically by about 30–40 per cent at 400 μm. This moderate increase would not affect any of our conclusions.

4.2 The radiative effect of SMBHs

Figs 5 and 6 highlight the radiative contribution of the SMBHs particles to the SEDs. The former one shows a comparison of the SEDs obtained with or without their effect for a couple of clusters seen at $z = 1$ and 2. Also, the SEDs are computed for two very different AGN templates (shown in Fig. 1; see Section 3). The latter figure displays the median ratio, the 25 per cent and the 75 per cent percentiles of the predicted fluxes including or excluding the radiative effect of AGNs, for all the sample. We note explicitly that in both cases, we are considering the same simulations in which the AGN feedback is included. Usually, in the spectral ranges between 0.1–1 μm and 15–100 μm rest frame, we found that the AGN activity boosts the integrated flux by a fraction ranging from ∼10 to 50 per cent at $z = 2$. Moreover, the effect tends to decrease with decreasing redshift, being often negligible at $z = 1$. However, in the far-UV at $\lambda \lesssim 0.1$ μm and in the near-IR at $2\ \mu m \lesssim \lambda \lesssim 15$ μm its contribution becomes more significant. In the former regime, this is due to the fact that QSOs are believed to emit a significantly harder spectrum than the stars below the Lyman limit, but the detailed result is strongly dependent on the adopted AGN template (this is the main reason why this range is not shown in Fig. 6). In the latter spectral regime, the reason is that only very concentrated

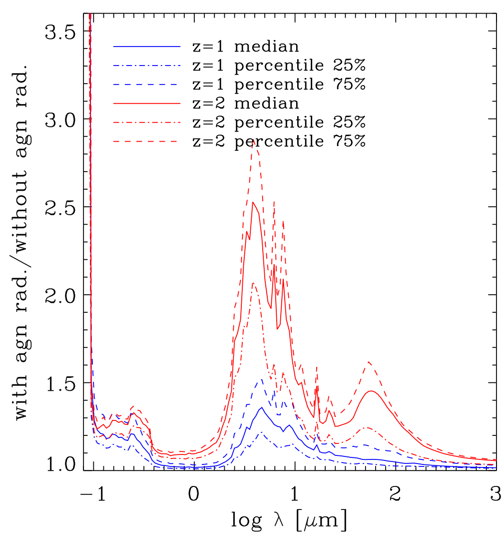

Figure 6. Ratio of the predicted fluxes including or excluding the radiative effect of AGNs, as a function of wavelength λ (rest frame), for our standard choice of GRASIL-3D parameters. Above ∼100 μm the difference is in most cases ≲ 25 per cent, decreasing with increasing λ.

and extremely luminous sources may produce an interstellar radiation field so intense to heat dust grains at $T \sim 1000$ K, which is required to get thermal emission peaking at λ a few μm. As a result, at $\lambda \sim 3$ μm, the AGNs often boost the predicted flux by a factor of a few. On the other hand, at $\lambda \gtrsim 100$ μm rest frame, the radiative effect of SMBH particles amounts to less than 25 per cent, with our chosen (as well as any reasonable) AGN SED template.

4.3 Sub-mm properties of the clusters

In the previous sections, we have seen that in the far-IR $\lambda \gtrsim 100$ μm the uncertainties introduced by the sub-resolution modelling of the radiative transfer in the MCs are negligible. The dust emission is

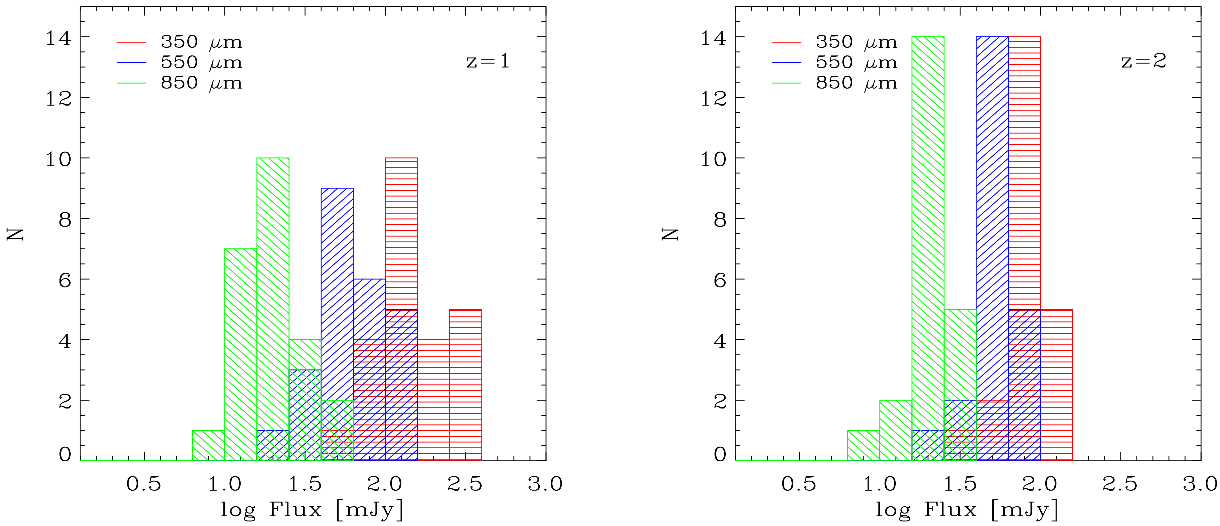

Figure 7. Distributions of the predicted fluxes from our sample of simulated clusters, within the *Planck* beam (∼5 arcmin FWHM) in the 350, 550 and 850 μm HFI bands (857, 545 and 353 GHz, respectively). The four candidate protoclusters selected by Clements et al. (2014) have photometric redshift of 0.76, 1.04, 2.05 and 2.26 and 350 μm HFI fluxes of 1100, 810, 1250 and 1240 mJy, i.e. close to the right bound of these plots. However, these fluxes are believed to be overestimated by a factor of 2 to 3 due to selection bias. See text for details and discussion.

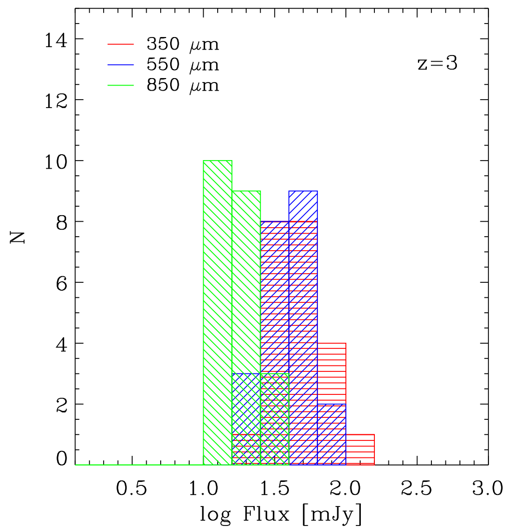

Figure 8. Same as Fig. 7, but at $z = 3$.

mostly powered by star formation with a tiny contribution from AGN activity. These are interesting points in view of the efficiency of far-IR/sub-mm surveys in detecting high-z objects in a violent, dust obscured, star-forming phase (e.g. Coppin et al. 2006, and references therein). Indeed, it has been proposed to take advantage of large area surveys performed in this spectral region to uncover pristine evolutionary phases of cluster regions, undergoing simultaneous starbursts (e.g. Negrello et al. 2005).

In this vein, Clements et al. (2014) have recently reported the potential detection of four clusters of dusty, star-forming galaxies at photometric redshift 0.76, 1.04, 2.05 and 2.26 by examining the *Herschel*-SPIRE images of Planck Early Release Compact Source Catalog (Planck Collaboration VII 2011) sources over an area of about 90 deg^2. With our panchromatic computation of the expected SED of the most massive cluster regions simulated in a large cosmological box, it is interesting to check to what extent these detections can be explained by our simulations. In this respect, it is worth pointing out that the comoving volume encompassed by the 90 deg^2 area over the $z = 0.76 - 2.3$ redshift range is of about 0.6 h^{-1} Gpc^3 for the adopted cosmology, thus smaller than the comoving volume of the parent simulation.

The measured *Planck* fluxes of the four cluster are all of the order of $\sim 10^3$ mJy at 350 μm (857 Ghz). However, as mentioned by the authors themselves, it must be taken into account that *Planck* fluxes fainter than 1.3 Jy are *flux-boosted* due to the well-known selection bias of faint sources sitting on top of positive noise (Herranz et al. 2013). Indeed, they found that the sum of the fluxes of the *Herschel* sources in the *Planck* beam are typically lower by a factor 2–3. Histograms of the predicted fluxes in the *Planck* bands for our sample of mock clusters are shown in Figs 7 and 8. The median expected flux is of about 131 and 85 mJy at $z = 1$ and 2, respectively, but there are cases reaching ∼300 and 100 mJy, respectively. Thus, we can conclude that the expected fluxes could marginally explain those reported by Clements et al. for the two sources $z \sim 1$, assuming a somewhat generous flux boosting. On the contrary, they fail to do so by a significative factor $\gtrsim$3–4 for the other two sources at $z \sim 2$. Indeed, while Clements et al. (2014), by considering the sum of the fluxes of *Herschel* sources within the *Planck* beam, estimate for their two $z \simeq 2$ clumps SFRs of at least[3] $\sim 2.9 \times 10^3$ and 7×10^3 M$_\odot$ yr^{-1}. By converse, none of our simulated cluster has an SFR exceeding 1700 M$_\odot$ yr^{-1} within the same beam (1300 M$_\odot$ yr^{-1} within the virial radius), with median value of 1000 M$_\odot$ yr^{-1} (800 M$_\odot$ yr^{-1} within the virial radius), as measured directly on the simulation output (see Fig. 9). It is also interesting to point out that very recently Dannerbauer et al. (2014), using APEX-LABOCA

[3] For consistency, we decreased these numbers by a factor of 1.7 with respect to those reported by Clements et al. (2014), since they uses a calibration of the relationship between total IR luminosity and SFR based on a Salpeter IMF, while our simulations adopt a more top heavy Chabrier IMF (see also footnote 1). However, Clements et al. claims that their SFRs are likely to be underestimated by a factor between 1.3 and 2. Note also that, had we adopted a Salpeter IMF in the simulations, both the SFR level would be slightly reduced due to lower recycled fraction, and the expected flux for a given SFR would be decreased, worsening both discrepancies.

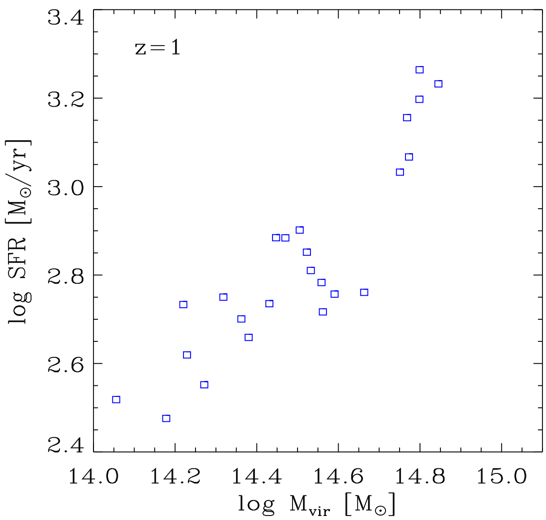

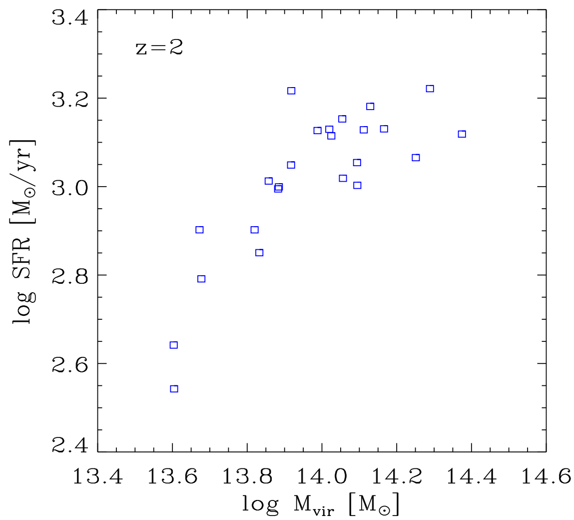

Figure 9. SFR as a function of virial mass for the sample of simulated clusters, at $z = 1$ (left) and $z = 2$ (right). The SFR is calculated including all gas particles within a box of 2000 kpc, close to the *Planck* HFI beam at both redshift.

observations at 870 µm, determined an SFR of $\gtrsim$6300 $M_\odot$ yr^{-1} within a region of the same size ~2 Mpc, around the protocluster region traced by the *spiderweb* radiogalaxy at $z = 2.16$, similar to that estimated by Clements et al., for their clumps at $z \sim 2$. We recall that, as discussed in Section 4.2, the contribution from AGN power to the flux in the spectral region covered by *Planck* is minimal for our simulated clusters. On the other hand, for the other two observed clumps, whose photometric redshifts are 0.76 and 1.04, their SFR estimates, again corrected downwards to our adopted Chabrier IMF, are $\gtrsim$350 and 950 $M_\odot$ yr^{-1}, respectively. These figures are thus not inconsistent with the SFRs in our sample at $z = 1$, whose median is 570 and maximum 1700 $M_\odot$ yr^{-1}.

Fig. 10 shows the contribution expected from our simulated clusters to the cumulative number counts, as unresolved sources, in the *Planck* HFI bands. They have been computed by integrating in redshift the luminosity functions evaluated at several redshifts between 0.5 and 3. As expected from the previous discussion, they do not show up at all at flux levels of the order of 1 Jy and in order to find a few clusters over an area of ~90 deg^2, as reported by Clements et al. (2014), it would be necessary, according to our computations, to reach much lower sensitivities, ~100 mJy at 350 µm. This is far too low even for the typical sensitivity ~0.7 Jy of the final Planck catalogues of compact sources (Planck Collaboration XXVIII 2014). It may be worth pointing out that Negrello et al. (2005), exploiting the simple semi-analytic model (SAM) by Granato et al. (2004) for the co-evolution of spheroids and QSO, which provided a good match to the sub-mm number counts available at that time, estimated, for an instrument with the resolution of *Planck*/HFI, surface densities of 850 µm sources in good keeping with the findings by Clements et al. (2014).[4] Furthermore, from the observational point of view, these finding seems to be strengthened by a more recent combined analysis of much larger portions of the sky observed by *Planck* and *Herschel* (Planck Collaboration XXVII 2015). In this case, hundreds of overdensities of high-z galaxies have been identified, which may be interpreted as protoclusters characterized by typical global SFR of the order of several thousands $M_\odot$ yr^{-1}.

Fig. 9 highlights that our sample of simulated cluster regions is characterized by a strong correlation between the instantaneous virial mass and the SFR, computed within a box matching the *Planck*-HFI beam, both at $z = 1$ and 2. We find a similar well-defined correlation between the SFR at any interesting z and the *final* virial mass, on which the selection of the sample is based (Section 2.1). As a consequence, it seems very unlikely that, extending our study to lower mass clusters, we could find systems featuring high-z SF activity as intense as that hinted by the recent observations and never attained by our objects.

In Fig. 11, we show the predicted $z = 2$ images in the *Herschel*-SPIRE 350 µm band for two cluster regions. These are the two regions characterized by the highest SFR in our sample at that redshift, ~1600 $M_\odot$ yr^{-1} within the box, and have been convolved with a Gaussian PSF of 25 arcsec full width at half-maximum (FWHM), corresponding to the telescope diffraction limit. As can be judged by these maps, the brightest simulated clusters are expected to produce at most 2–3 individual sources with a flux in the beam slightly above the *Herschel* confusion limit at this wavelength (~6 mJy) (Nguyen et al. 2010).

In conclusion, it would be very difficult, if not impossible, to uncover and study structures similar to those predicted by our simulations with present-day FIR and sub-mm space facilities.

As we mentioned before, we have also simulation runs with AGN feedback switched off. In this case the predicted SFRs, and correspondingly the expected fluxes in the *Herschel* bands, are typically higher by a factor of ~2 and 1.5 at redshift 1 and 2, respectively. These numbers would be in better agreement with the figures quoted by Clements et al. (2014), albeit still too low at $z \sim 2$. Moreover, it is well known that without some treatment of this astrophysical process, cosmological simulations overpredict the amount of baryons converted into stars, particularly in massive systems, by about one order of magnitude (see for instance Ragone-Figueroa et al. 2013, and references therein).

One possibility to increase the predicted fluxes would be to adopt a more top heavy IMF. However, in order to get an increase by a factor of a few, as required in particular by the finding of Clements et al. (2014), the IMF should be quite extreme, similar to the flat

[4] See fig. 14 in Clements et al. (2014), bearing in mind that they dubbed *numerical simulation* a Monte Carlo realization of sub-mm sky, again based on the Granato et al. (2004) SAM.

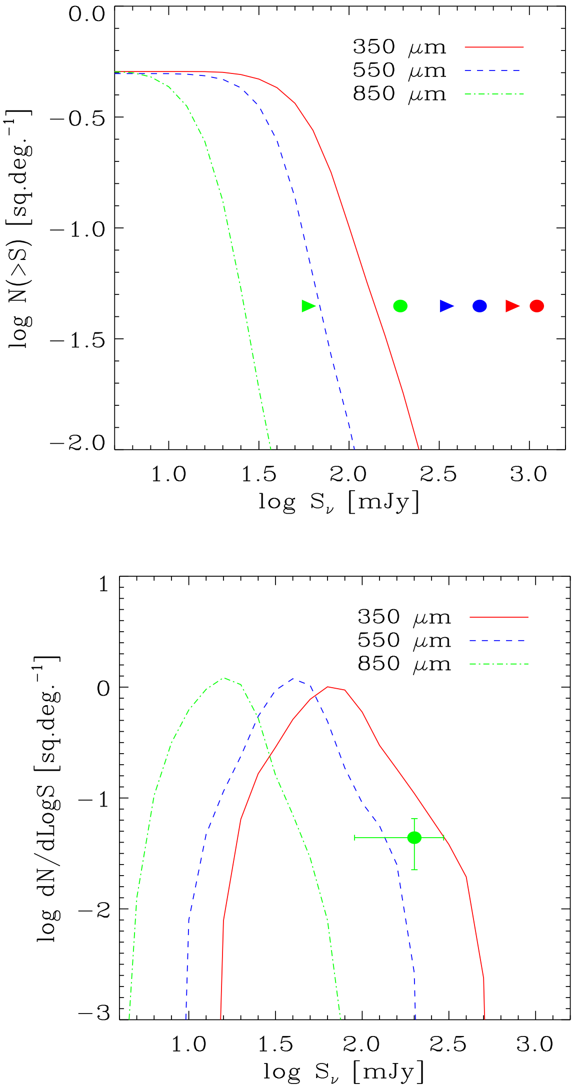

Figure 10. Expected contribution to the cumulative and differential number counts in the *Planck* HFI bands from the simulated clusters considered in this work, namely all clusters whose final virial mass $\gtrsim 1 \times 10^{15}\, h^{-1}\, M_\odot$, treated as unresolved sources. In the upper panel, the coloured circles (triangles) mark the position corresponding to the average (minimum) fluxes and the number density suggested by the four *Planck* clumps detected by Clements et al. (2014) over an area of 90 deg^2. In the lower panel, the circle with error bars is the estimate given by the these authors at 850 μm.

IMF postulated by the Durham SAM (during bursts) to reproduce the sub-mm number counts (Baugh et al. 2005). We have verified that in this case the SFR would be only slightly modified, because two competing effects almost cancel each other: more gas recycling and faster chemical enrichment on one side, and stronger SNae feedback on the other side. In the deepest developing potential wells yielding to the formation of the most massive clusters, we found, according to our prescriptions, some prevalence of the former effect, causing an increase of SFR by no more than 10–20 per cent. However, adopting such an extreme IMF, the predicted flux for a given SFR at $\lambda > 100\,\mu$m rest frame can increase by a factor of a few, the exact value depending on the star formation history. There are some hints of IMFs more top heavy than Chabrier in violently star-forming environments (but also for the opposite), but nothing approaching such an extreme IMF has ever been observed. Moreover, later studies have shown that this quite ad hoc assumption leads to a few remarkable problems in the context of the Durham SAM (for a discussion see Casey, Narayanan & Cooray 2014). It seems therefore unlikely that the difficulty highlighted in this section can be entirely solved by the adoption of a different IMF in our simulations.

5 SUMMARY AND CONCLUSIONS

In this work, we have post-processed a sample of cosmological zoom-in simulations following the formation of the 24 most massive galaxy clusters selected from a parent simulation of box size of 1 h^{-1}Gpc. The final virial mass of the clusters ranges from $\simeq$1 to $3 \times 10^{15}\, h^{-1}\, M_\odot$. The post-processing consists of performing radiative transfer computations with the GRASIL-3D code (Domínguez-Tenreiro et al. 2014) including dust reprocessing, in order to predict the IR properties of the forming clusters during the most active star-forming phases. We have implemented in GRASIL-3D a treatment of the radiative contribution due to AGN activity, consistent with the prescriptions adopted in the simulation for the AGN feedback. The latter is widely recognized as a key ingredient to limit the over-production of stars in massive haloes. The expected contribution to the IR emission from accretion power could be significant at $\lambda \lesssim 100$ μm, but minor or negligible at $\lambda \gtrsim 100$ μm. However, going to shorter and shorter wavelengths, the exact budget becomes progressively dependent on the adopted GRASIL-3D assumptions.

We have demonstrated that during the early phases of assembly of massive galaxy clusters our simulations do not reach far-IR luminosities high enough, by a factor at least of a few, to account for the reported discovery of four high-z, massively star forming clusters by Clements et al. (2014), over an area of about 90 deg^2 in the *Planck* satellite survey. Since we have shown that this conclusion is very robust with respect to any reasonable variation of the assumptions required to perform the dust emission computations and that the possible contribution to the overall emission from AGN is small in this spectral regime, the problem directly translates to *insufficient peaks* of star formation activity in the simulations at early epochs. This problem becomes more puzzling taking into account that the same simulations *overpredict* the final stellar mass in BCGs hosted by massive clusters at $z = 0$, by a factor of a few (Ragone-Figueroa et al. 2013).

High-redshift SFRs can be increased in numerical simulations. Improving the resolution would already boost the SFR to some extent (e.g. Borgani et al. 2006), but still not enough to eliminate the tension between observations and the models. Also, it would be possible to re-calibrate the sub-grid prescriptions for the baryon physics. However, it appears very difficult to enhance the SFR at high redshifts without also increasing the final mass of simulated BCGs, thus worsening the above-mentioned disagreement. Indeed, there have been already reports of a paucity of strong starbursts in recent cosmological simulations, once their sub-resolution physics is calibrated to reproduce other constraints (e.g. Sparre et al. 2015). These violent star formation events would be required to explain the statistical properties of the general population of sub-mm selected galaxies (SMGs). We wish to address this issue in the near future, by applying the GRASIL-3D post-processing described in this paper to a forthcoming hydrodynamical simulation of an entire (rather than just zooms of the massive cluster regions) cosmological box, including sub-resolution physics. This would provide new clues on the ongoing debate on the use of SMGs to trace the assembly of massive structures at high z (e.g. Miller et al. 2015, and references therein).

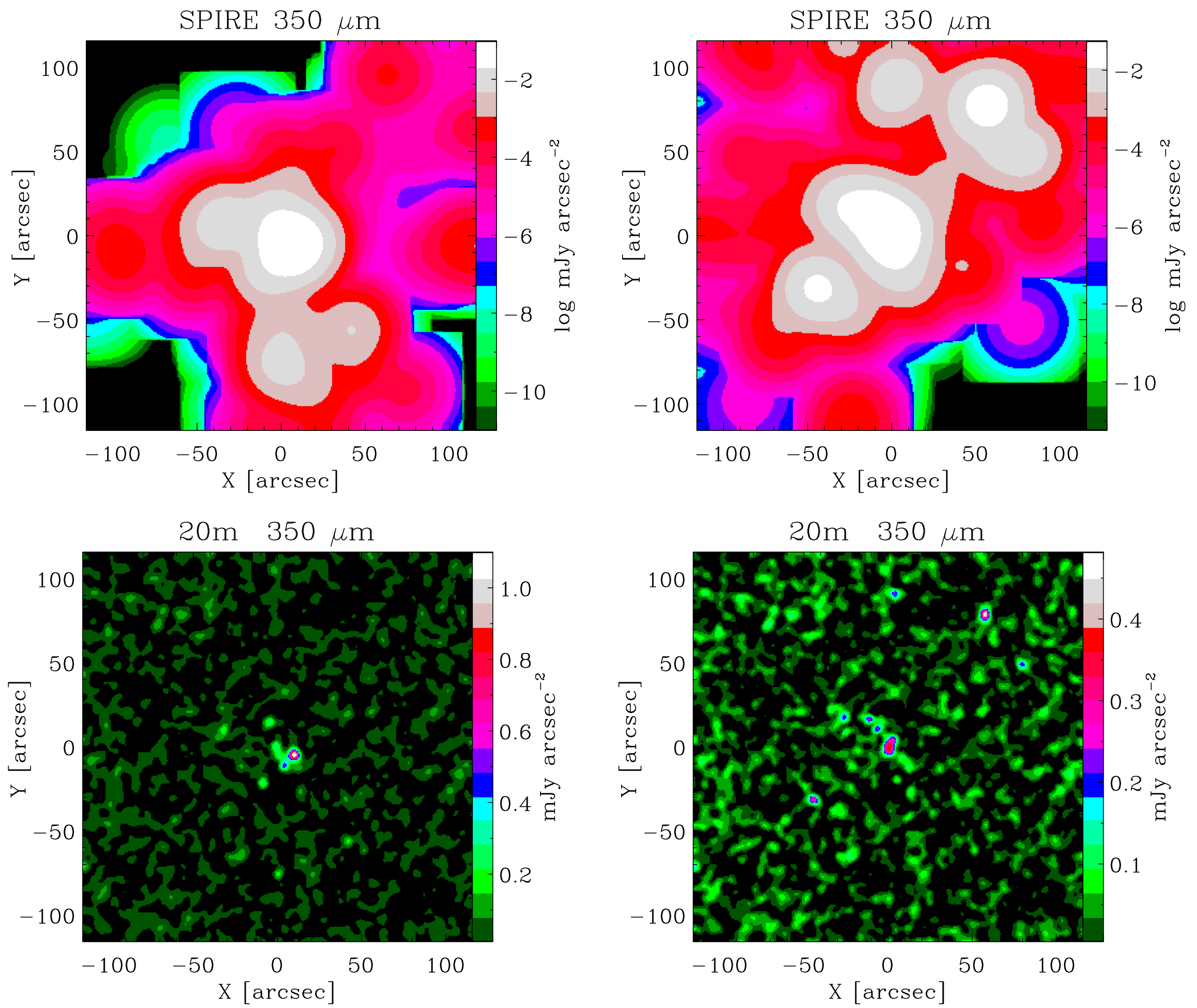

Figure 11. 350 μm (observed) GRASIL-3D images for the two cluster regions (left-hand and right-hand columns) at $z = 2$ having the highest SFR (at that redshift) in our sample, namely ∼1600 $M_{\odot}$ yr^{-1} within the box. The box physical size is 2000 kpc, close to the *Planck* HFI beam at $z = 2$. The images in the top row have been convolved with a Gaussian PSF of 25 arcsec FWHM, corresponding to the *Herschel* telescope diffraction limit. We expect at most 2–3 individual sources with a flux in the beam above the *Herschel* confusion limit at this wavelength (∼6 mJy). In the bottom row, the images include a Gaussian noise of 0.1 mJy arcsec^{-2} 1σ, and are convolved with a PSF of 3.1 arcsec FWHM. This resolution can be achieved by a 20 m single dish telescope (see Sauvage et al. 2014).

Moreover, recent observations suggest a picture according to which the $z \gtrsim 1.5$ population of galaxy (proto)clusters contains examples with both extreme (e.g. Tran et al. 2010; Clements et al. 2014; Dannerbauer et al. 2014; Santos et al. 2014, 2015) as well as very low star formation activity (e.g. Tanaka et al. 2013; Kubo et al. 2015), while in our simulated clusters these two opposite situations are clearly underrepresented. It seems that the bulk of star formation in the progenitors of real massive galaxy clusters occurred at higher rates, but lasted less than in our simulations.

These opposite tensions may indicate that the prescriptions adopted to describe the sub-resolution processes should be improved to better capture the relevant physics. Possibly, if the situation hinted by the growing data set on (proto)clusters at $z \gtrsim 1$ is confirmed, the interplay between the feedback schemes and the star formation model should yield overdense regions characterized by both higher and lower star formation levels than attained in current simulations, while avoiding an overproduction of stars over the assembly history of the most massive cluster galaxies. It is conceivable that an early phase of positive feedback during the development of AGN activity (e.g. Silk 2013) and/or a longer delay between the most violent episodes of star formation and the onset of efficient AGN quenching (e.g. Granato et al. 2004) could be part of a more realistic modelling.

Finally, we notice that since our prescriptions for the baryonic sub-grid physics, apart minor variations, are quite standard in present day cosmological simulations, we expect that our findings would apply to most of them in the same halo mass regime.

ACKNOWLEDGEMENTS

We thank the referee Dave Clements for his constructive comments, which substantially helped to improve the quality of the paper. We acknowledge useful exchange of ideas and information with Gianfranco De Zotti, Herve Dole, Samuel Farrens, Chris Hayward, Paolo Tozzi and Joana Santos. GLG acknowledges warm hospitality by IATE-Córdoba during the development of this work. We thank Volker Springel for making available to us the non-public version of the GADGET3 code. Simulations have been carried out at the CINECA supercomputing Centre in Bologna, with CPU time assigned through ISCRA proposals and through an agreement with University of Trieste. CRF acknowledges founding from the Consejo Nacional de Investigaciones Científicas y Técnicas de la República Argentina (CONICET), by the Secretaría de Ciencia y Técnica de la Universidad Nacional de Córdoba (SeCyT) and by the Fondo para la Investigación Científica y Tecnológica (FonCyT). This work has been supported by the PRIN-MIUR 201278X4FL Evolution of cosmic baryons funded by the Italian Ministry of Research, by the PRIN-INAF09 project Towards an Italian Network for Computational Cosmology, and by the INDARK INFN grant, by the MICINN and MINECO (Spain) through the grants AYA2009-12792-C03-03 and AYA2012-31101 from the PNAyA and by the European Commission's Framework Program 7, through the International Research Staff Exchange Program LACEGAL. AO was financially supported through an FPI contract from AYA2009-12792-C03-03.

REFERENCES

Baugh C. M., Lacey C. G., Frenk C. S., Granato G. L., Silva L., Bressan A., Benson A. J., Cole S., 2005, MNRAS, 356, 1191
Bonafede A., Dolag K., Stasyszyn F., Murante G., Borgani S., 2011, MNRAS, 418, 2234
Borgani S. et al., 2006, MNRAS, 367, 1641
Bryan G. L., Norman M. L., 1998, ApJ, 495, 80
Camps P., Baes M., 2015, Astron. Comput., 9, 20
Casey C. M., Narayanan D., Cooray A., 2014, Phys. Rep., 541, 45
Chabrier G., 2003, PASP, 115, 763
Chakrabarti S., Whitney B. A., 2009, ApJ, 690, 1432
Clements D. L. et al., 2014, MNRAS, 439, 1193
Cooper M. C. et al., 2008, MNRAS, 383, 1058
Coppin K. et al., 2006, MNRAS, 372, 1621
Crain R. A. et al., 2015, preprint (arXiv:1501.01311)
Dannerbauer H. et al., 2014, A&A, 570, A55
Davis M., Efstathiou G., Frenk C. S., White S. D. M., 1985, ApJ, 292, 371
Domínguez-Tenreiro R., Obreja A., Granato G. L., Schurer A., Alpresa P., Silva L., Brook C. B., Serna A., 2014, MNRAS, 439, 3868
Draine B. T., Lee H. M., 1984, ApJ, 285, 89
Efstathiou A., Rowan-Robinson M., 1995, MNRAS, 273, 649
Elbaz D. et al., 2007, A&A, 468, 33
Fassbender R. et al., 2014, A&A, 568, A5
Gobat R. et al., 2013, ApJ, 776, 9
Granato G. L., Danese L., 1994, MNRAS, 268, 235
Granato G. L., Danese L., Franceschini A., 1997, ApJ, 486, 147
Granato G. L., Lacey C. G., Silva L., Bressan A., Baugh C. M., Cole S., Frenk C. S., 2000, ApJ, 542, 710
Granato G. L., De Zotti G., Silva L., Bressan A., Danese L., 2004, ApJ, 600, 580
Guo Q. et al., 2011, MNRAS, 413, 101
Hatch N. A., Kurk J. D., Pentericci L., Venemans B. P., Kuiper E., Miley G. K., Röttgering H. J. A., 2011, MNRAS, 415, 2993
Hayashi M., Kodama T., Koyama Y., Tadaki K.-I., Tanaka I., 2011, MNRAS, 415, 2670
Herranz D. et al., 2013, A&A, 549, A31
Hilton M. et al., 2010, ApJ, 718, 133
Hoenig S. F., 2013, preprint (arXiv:1301.1349)
Hopkins P. F., Kereš D., Oñorbe J., Faucher-Giguère C.-A., Quataert E., Murray N., Bullock J. S., 2014, MNRAS, 445, 581
Inagaki T., Lin Y.-T., Huang H.-J., Hsieh B.-C., Sugiyama N., 2015, MNRAS, 446, 1107
Johansson P. H., Naab T., Ostriker J. P., 2012, ApJ, 754, 115
Jones A., 2014, preprint (arXiv:1411.6666)
Jonsson P., Groves B. A., Cox T. J., 2010, MNRAS, 403, 17
Kravtsov A. V., Borgani S., 2012, ARA&A, 50, 353
Kubo M., Yamada T., Ichikawa T., Kajisawa M., Matsuda Y., Tanaka I., 2015, ApJ, 799, 38
Li Y. et al., 2008, ApJ, 678, 41
Lidman C. et al., 2012, MNRAS, 427, 550
Lin Y.-T., Brodwin M., Gonzalez A. H., Bode P., Eisenhardt P. R. M., Stanford S. A., Vikhlinin A., 2013, ApJ, 771, 61
Mei S. et al., 2009, ApJ, 690, 42
Miller T. B., Hayward C. C., Chapman S. C., Behroozi P. S., 2015, preprint (arXiv:1501.04105)
Negrello M., González-Nuevo J., Magliocchetti M., Moscardini L., De Zotti G., Toffolatti L., Danese L., 2005, MNRAS, 358, 869
Nguyen H. T. et al., 2010, A&A, 518, L5
Obreja A., Brook C. B., Stinson G., Domínguez-Tenreiro R., Gibson B. K., Silva L., Granato G. L., 2014, MNRAS, 442, 1794
Pier E. A., Krolik J. H., 1993, ApJ, 418, 673
Planck Collaboration VII, 2011, A&A, 536, 7
Planck Collaboration XXVIII, 2014, A&A, 571, A28
Planck Collaboration XXVII, 2015, A&A, submitted
Planelles S., Borgani S., Fabjan D., Killedar M., Murante G., Granato G. L., Ragone-Figueroa C., Dolag K., 2014, MNRAS, 438, 195
Polletta M. et al., 2007, ApJ, 663, 81
Ragone-Figueroa C., Granato G. L., Murante G., Borgani S., Cui W., 2013, MNRAS, 436, 1750
Richards G. T. et al., 2006, ApJS, 166, 470
Rigby E. E. et al., 2014, MNRAS, 437, 1882
Santos J. S. et al., 2011, A&A, 531, L15
Santos J. S. et al., 2014, MNRAS, 438, 2565
Santos J. S. et al., 2015, MNRAS, 447, L65
Sauvage M. et al., 2014, Proc. SPIE, 9143, 91431B
Silk J., 2013, ApJ, 772, 112
Silva L., Granato G. L., Bressan A., Danese L., 1998, ApJ, 509, 103
Sparre M. et al., 2015, MNRAS, 447, 3548
Springel V., 2005, MNRAS, 364, 1105
Springel V., Di Matteo T., Hernquist L., 2005, MNRAS, 361, 776
Stott J. P., Collins C. A., Burke C., Hamilton-Morris V., Smith G. P., 2011, MNRAS, 414, 445
Strazzullo V., Pannella M., Owen F. N., Bender R., Morrison G. E., Wang W.-H., Shupe D. L., 2010, ApJ, 714, 1305
Strazzullo V. et al., 2013, ApJ, 772, 118
Tanaka M. et al., 2013, ApJ, 772, 113
Tormen G., Bouchet F. R., White S. D. M., 1997, MNRAS, 286, 865
Tran K.-V. H. et al., 2010, ApJ, 719, L126

This paper has been typeset from a TEX/LATEX file prepared by the author.